Friction **12**(10): 2281–2297 (2024)
https://doi.org/10.1007/s40544-024-0871-x
ISSN 2223-7690
CN 10-1237/TH

RESEARCH ARTICLE

An inorganic–organic hybrid CQDs@PVP lubricant additive: Achieving low friction and wear in PEG and water

Tao YANG[1,2,3,†], Xiaozhen WANG[4,†], Huanchen LIU[1], Qin ZHAO[1], Kuiliang GONG[1], Weimin LI[1], Yongmin LIANG[2,*], Xiaobo WANG[1,*]

[1] *State Key Laboratory of Solid Lubrication, Lanzhou Institute of Chemical Physics, Chinese Academy of Sciences, Lanzhou 730000, China*

[2] *State Key Laboratory of Applied Organic Chemistry, College of Chemistry and Chemical Engineering, Lanzhou University, Lanzhou 730000, China*

[3] *Center of Materials Science and Optoelectronics Engineering, University of Chinese Academy of Sciences, Beijing 100049, China*

[4] *Zibo Innovation Center of High-end Synthetic Lubricating Materials, Zibo 255000, China*

Received: 28 September 2023 / Revised: 27 November 2023 / Accepted: 05 January 2024

© The author(s) 2024.

Abstract: High-temperature lubrication has always been a hot topic in the lubricant and grease industry, and is also an essential concern in the high-end equipment sector to be addressed. Carbon quantum dots (CQDs) are an emerging material widely applied in the field of lubrication, owing to their exceptional lubricity and high load-bearing capacity. However, the vulnerability of CQDs to oxidation in air and reduced stability dramatically restrict their high-temperature application capability. In this study, a nanocomposite of amphiphilic polyvinyl pyrrolidone (PVP) homopolymer with excellent lubricating properties and thermal stability, which is hydrogen bonded to CQDs (CQDs@PVP), was designed to achieve low friction and wear of lubricants at high temperatures. The CQDs@PVP are consistently dispersed in both PEG400 and water, and exhibit superior lubricity compared to unmodified CQDs at high temperatures (ranging from 200–150 °C and 90–50 °C). Meanwhile, the dense carbon film on the wear surface and the chemically reactive film of iron compounds directly contribute to the enhanced lubrication performance. These analytical results demonstrate the powerful candidacy of CQDs@PVP as a lubrication additive and promote future high-temperature applications of CQDs in industrial production.

Keywords: high temperature lubricants; amphiphilic lubrication additives; CQDs@PVP; lubrication properties; carbon film

1 Introduction

Abominable ambient conditions of extreme operating situations such as high temperature, heavy load, and express speed are the root elements of friction and wear, which cause mechanical deterioration, shorten device life, and inhibit the development of energy, economy and environment [1–5]. Lubricants are a valid implement to accomplish minimum frictional wear between machines to overcome the issues of industrial equipment failure [6, 7]. Nevertheless, mineral oil, vegetable oil and other base oils are insufficient to fulfill the operating conditions of most equipment [8]. Properly and rationally selecting additives which are the essence of contemporary premium lubricants, allow the physical and chemical properties of lubricants to be refined and endowed with exceptional performance to satisfy higher requirements [9, 10]. In recent years, the exploration of lubrication additives has concentrated primarily on various dimensional

† Tao YANG and Xiaozhen WANG contributed equally to this work.

* Corresponding authors: Yongmin LIANG, E-mail: liangym@lzu.edu.cn; Xiaobo WANG, E-mail: wangxb@licp.cas.cn

nanomaterials, such as zero-dimensional tungsten disulfide (WS_2) quantum dots [11], one-dimensional carbon nanotubes (CNTs) [12], and two-dimensional layer crystal structure of molybdenum disulfide (MoS_2) [13], etc.

The zero-dimensional carbon quantum dots (CQDs) of emitting bright fluorescent light have drawn widespread attention and intensive investigation from researchers since they were initially discovered in 2004 [14]. The researchers made significant progress in their studies on the properties and applications of CQDs, such as chemical sensors [15], biological imaging [16], phototherapy technology [17], drug carrier [18], lubrication additive [19], and chemical catalysis [20], as it possesses a broad range of raw materials sources, lower preparation costs, and tremendous advantages in the field of material fabrication [21]. Currently, CQDs are commonly employed as a single additive in lubrication because of their excellent surface chemical activity, specific surface energy, and biocompatibility [22]. Especially the primary applications of CQDs are high-performance friction reduction and anti-wear additives in conventional environments. However, the lubrication capability under extreme operating conditions, including high temperature and lubrication stability among multiple environmental considerations like high load, is poor, which reduces base-oil mechanical performance and restricts their practical application [23]. The drawbacks of CQDs, therefore, need to be adequately considered, which can be optimized and tuned to various lubrication conditions and demands to achieve enhanced macroscale lubricity through chemical modification [24]. Polyvinyl pyrrolidone (PVP) is a non-toxic, odorless, biocompatible, amphiphilic polymeric material that is widely applied as a lubricant [25], stabilizer [26], dispersant [27], thickening agent [28], and drug carrier [29]. PVP serves as a surfactant to enhance the lubricating properties and reduce the friction, wear, and energy consumption of base oils under extremely conditions, which improves the efficiency and service life of mechanical components [30]. Simultaneously, the carbonyl group of PVP and the hydroxyl group on the surface of the CQDs combine to form a hydrogen bonding interaction, allowing a robust interaction between PVP and the CQDs to produce a stable composite material [31]. The hydrogen bonding promotes molecular interactions between liquids and decreases viscosity, thus increasing the fluidity and consistency of the lubrication. Consequently, the combination of CQDs and PVP (CQDs@PVP) in the base oil can transform its interfacial properties and molecular structure to avoid friction, wear and corrosion, providing a potent safeguard to realize a strong lubrication effect.

In this work, we have taken a brief chemical modification to compound the CQDs synthesized by pyrolysis with PVP, which exhibits excellent friction reduction and anti-wear properties at high temperatures and loads. In the meantime, various characterizations were carried out to identify the physical morphology and chemical structure of CQDs@PVP compounds as well as the countenance of the tribo-pairs surface after the tribological test. In contrast with most polymer additives, CQDs@PVP has demonstrated extremely stable dispersion in PEG-400 and water, which can stand for 180 days without sedimentation. It is considered the electrostatic interaction of functional groups, such as carboxyl groups in the molecular structure with polar solvents. Moreover, CQDs and PVP, which possess high specific surface energy and strong surface adsorption capacity, have significantly improved interfacial activity and adsorption of lubricants, and decreased the direct contact between tribopairs to consolidate the lubrication effect. These explorations may widen the ambits of extreme operating conditions lubrication additives available and have extensive application potential in high-end equipment and precision instrument.

2 Materials and methods

2.1 Materials

The citric acid (CA, ≥99.5%) was purchased from Macklin, and polyvinyl pyrrolidone K30 (PVP, CP) was purchased from Shanghai Shanpu Chemical Co., China. Petroleum ether (PE, AR) was purchased from Tianjin Fuyu Fine Chemical Co., China, and ethanol absolute (EtOH, AR) was purchased from Chengdu Chron Chemical Co., China. Polyethylene glycol

(PEG400, AR) and ethyl acetate (EtOAc, AR) were obtained from Sinopharm Chemical Reagent. All experimental chemical reagents require no further purification prior to use. Dialysis bags (MD55-2000Da) were obtained from Yibo Biological Co., USA and needed to be treated in boiling water at 100 °C for 10 min before use.

2.2 Synthesis of CQDs@PVP

The CQDs were prepared *in situ* by the most commonly used pyrolysis method [32, 33]. Specifically, CA (5 g) was added into a 50 ml single-necked flask and submerged in an oil bath. Meanwhile, the phase change and color shift of CA particles was observed at 200 °C. The CA pellets were found to turn from solid to liquid, and the color of the product gradually changed from colorless and transparent to yellowish-orange as the heating process continued. At this point, the specimen was removed from the oil bath and cooled at room temperature for approximately 20 min. Add deionized water (100 mL) to the above system and stir for 30 min to disperse the mixture. The CQDs were extracted with EtOAc and then added with an equal amount of deionized water. The aqueous solution was poured into the treated dialysis bag for 24 h, with the water replaced every 8 h. At last, spin-drying the lyophilized dialysate yielded the CQDs product.

The CQDs (100 mg) powder was scattered into a mixed solution of PE and EtOH (60 mL, 20:1), then PVP (200 mg) was added to the mixture and transformed into a hydrothermal synthesis reactor under 120 °C for 6 h. The solution removed the excess raw materials between centrifugation and washing with deionized water, and the precipitate was dried in vacuum at 35 °C for 12 h to obtain powder of CQDs@PVP nanoparticle.

2.3 Tribological tests

The tribological tests were performed on Oscillating friction and wear tester (SRV-V, Optimol Grease) to evaluate the tribological properties of the blend with base oil and additives. The bearing steel ball (AISI 52100) with a diameter of 10 mm and hardness of 62±3 HRC was clamped on the upper fixture device to oscillate, sliding against the steel disc (AISI 52100) fixed on the bottom with the diameter Φ24×7.9 mm and hardness 62±3 HRC, which was sonicated for 10 min to clean the oil stain of the balls and discs by PE before each test. The test conditions of the PEG400 system were load 200 N, frequency 25 Hz, stroke 1 mm, running time 30 min, and temperature 150 to 200 °C. Unlike the PEG400 system, the elapsed time was 10 min at 80 °C and 90 °C considering that the aqueous solution evaporated under these conditions, and all testing conditions were identical except for the temperature of 50 to 70 °C.

Various quality fractions (0.5, 1.0, 1.5, and 2.0 wt%), of CQDs@PVP were added to PEG400 and water, respectively, and carried out for subsequent tribological tests with sonicated for 10 min. Meanwhile, CQDs were used as comparison samples to incorporate PEG400 and water in the same proportions, respectively. The balls and discs were wiped by EtOH, and dripped about two drops of mixture on the surface of the disc before tribological test began. All test conditions were set in advance, and the data for each second of operation was recorded on the test computer. After the test, the friction surface was washed with EtOH to remove the excess solution. All tests were repeated twice to guarantee the accuracy of the data.

2.4 Characterization

The physical morphologies of CQDs and CQDs@PVP nanoparticles were observed by the high-resolution transmission electron microscope (HR-TEM, Talos F200S, FEI), selected area electron diffraction (SAED, Talos F200S, FEI), and the energy spectrum scanning (Mapping, Tecnai G2 F20, FEI) demonstrated element distribution of the specimens. The Fourier transform infrared (FTIR) spectrometer (Tensor 27, Bruker) in the wavenumber range of 4,000–400 cm^{-1}, Ultraviolet and visible (UV-vis) spectrophotometry (TU-1810DSPC, Persee) in the wavelength range of 200–500 nm, and X-ray photoelectron spectroscopy (XPS, K-Alpha, Thermo Scientific) were conducted to proof chemical structure composition of CQDs@PVP nanoparticles. Thermo gravimetric analyzer (TGA, STA 449 F5 Jupiter, Netzsch) curves in the temperature range 40–800 °C under nitrogen atmosphere were used to characterize the practical composition of CQDs@PVP.

The morphologies of the wear surfaces on the steel

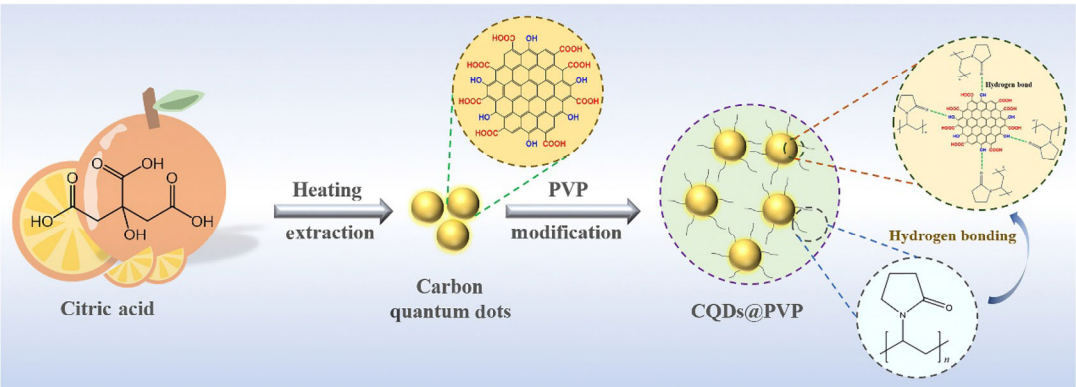
discs after friction were observed by optical microscope (OM, Axioscope 5, ZEISS) and scanning electron microscope (SEM, EVO 10, Zeiss). Correspondingly, the energy dispersive spectrometer (EDS, Xplore 15, Oxford Instruments) assembled in SEM was used to suggest the element distributions and approximate content of the worn scar. In addition, the non-contact three-dimensional (3D) optical surface profilometer (LEXT OLS5000, Alpha) was employed to observe 3D morphologies, wear volume, and depth of the wear tracks on the surface of steel discs sheet. Meanwhile, the phase composition of wear scar after friction at various temperatures was studied using a Raman spectrometer (RS, DXR2, Thermo Fisher). The X-ray photoelectron spectroscopy (XPS, K-Alpha$^+$, Thermo) was applied to demonstrate the formation of the tribofilm on the wear scar surface, and the radiation source with a power 150 W of the equipment is Al K alpha. Meanwhile, the test conditions were energy: 1,486.8 eV, illuminance area: 400 μm, tube voltage: 15 kV, tube current: 10 mA, and analysis chamber background vacuum: 2×10^{-9} mbar.

3 Results and discussion

3.1 Synthesis mechanism and physicochemical characterization of the CQDs@PVP

Scheme 1 depicts the synthesis mechanism and chemical structure schematic diagram of the CQDs and CQDs@PVP nanoparticles (NPs), which are prepared by pyrolysis and hydrothermal method, respectively. The CA was heated and extracted to obtain nano-sized (1–10 nm) CQD particles, and the PVP was modified on the surface of CQDs by chemical modification. The surface of the CQDs contained abundant hydroxyl and carboxyl groups that interacted with the carbonyl group of PVP to form hydrogen bonds, allowing for settled interactions between PVP and CQDs to create a stable CQDs@PVP composite [34]. Therefore, the high dispersion of PVP provided superior encapsulation and fixation of carbon quantum dots and improved the fluidity of the base oil, thereby effectively regulating and strengthening the lubricating properties. At the same time, the film on the surface of the CQDs@PVP served to reduce friction between the tribopairs and contributed to the protective effect of the surface lubrication layer.

To visualize the physical morphology of the CQDs and CQDs@PVP nanoparticles, the HR-TEM and mapping tests were carried out as shown in Fig. 1. The CQDs NPs (Figs. 1(a) and 1(b)) exhibited a homogeneously dispersed morphology except for individual particles, with a dimensional range of approximately 2.5 nm (illustration in Fig. 1(a)). Meanwhile, the inset in the green image frame of Fig. 2(b) clearly showed that the lattice spacing of CQDs was 0.21 nm, corresponding to the (100) crystal plane in the diffraction ring. Identically, the CQDs@PVP NPs (Figs. 1(c) and 1(d)) were further homogeneous quasi-spherical particles. With PVP modified on the CQDs surface, visible encapsulation shell structures from PVP could not be clearly observed due to the undersize of CQDs. However, the CQDs@PVP with an average size of about 3.0 nm increased by 0.5 nm compared to CQDs, which also indirectly proved the PVP modification of CQDs. The energy spectrum scanning element mapping (Figs. 1(e)–1(h)) showed



Scheme 1 Synthesis strategy and chemical structure schematic diagram of CQD and CQDs@PVP nanoparticles.

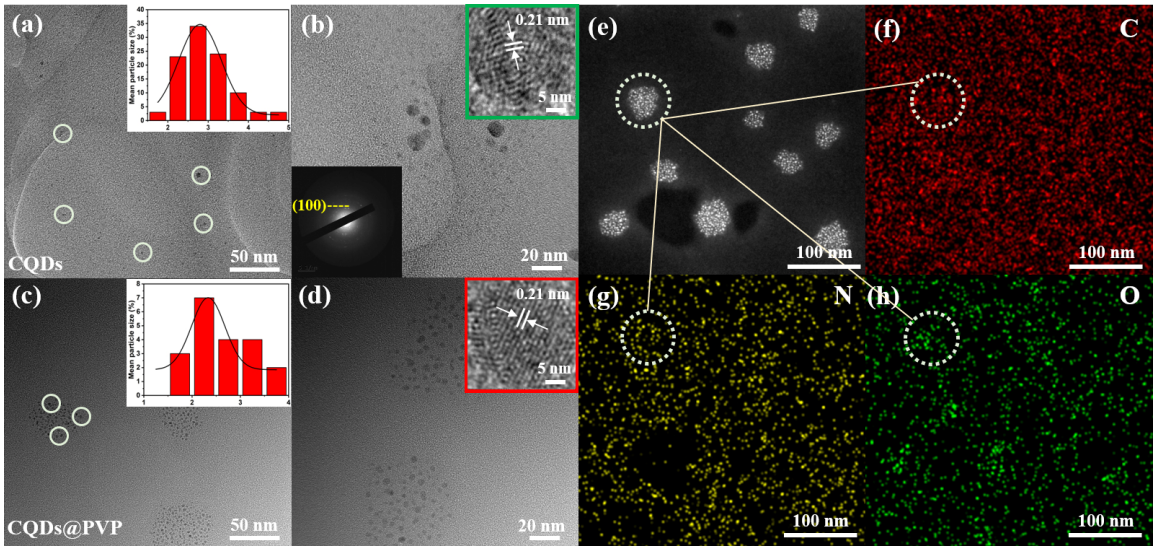


Fig. 1 Electron microscope characterization of CQDs and CQDs@PVP. TEM images of (a, b) CQDs and (c, d) CQDs@PVP. The insets show the average size and lattice spacing of (a) CQDs (embedded in the green frame) and (c) CQDs@PVP (embedded in the red frame), respectively. The HAADF image of (e) CQDs@PVP and EDS element mapping images of (f) C, (g) N, (h) O.

that elements C, O, and N from PVP displayed concentrated distribution (white dotted circles in the figures) and were evenly distributed around the surface of CQDs particles. Therefore, it revealed the excellent dispersion and the modification of PVP shell demonstrated the successful preparation of CQDs@PVP composite material.

The chemical structure of CQDs@PVP was inferred by FTIR (Fig. 2(a)) to determine the modification behavior of PVP. The characteristic peaks of CQDs at 3,465 and 1,409 cm^{-1} were ascribed to the stretching vibration of own hydroxyl bonds (ν_{OH}) and the deformation vibration of hydroxyl bonds (δ_{OH}) in the carboxyl group, respectively [35]. The stretching vibration of the carbonyl group ($\nu_{C=O}$) in –COOH was also present at peak 1,724 cm^{-1}. With the modification of PVP homopolymer, the emergence of the new peak at 1,443 cm^{-1} in CQDs@PVP was attributed to the N=O group, indicating the successful adhesion of the modifier to the CQDs surface. Additionally, compared with the hydroxyl and carbonyl group characteristic peaks of CQDs at 3,465 and 1,724 cm^{-1}, the absorption peaks of –OH and C=O at 3,440 and 1,651 cm^{-1} revealed the blueshift from the vibration frequency of the conjugate which was ascribed to the hydrogen bonds formation, suggesting the absorption frequency of both groups decreased, but the absorption intensity increased after the formation of the hydrogen bonds [36]. Simultaneously, the broadening of the vibrational bands on the hydroxyl peaks also indicated the hydrogen bond creation, implying the PVP homopolymer was grafted onto the surface of CQDs. Based on the above results, it appeared that CQDs@PVP composite material was successfully prepared.

The composition of the CQDs@PVP conjugate was estimated by TGA under a nitrogen atmosphere (Fig. 2(b)). As the temperature increased to 156 °C, the weight loss curve of CQDs began to appear at the inflection point which indicated the occurrence of thermal decomposition at the current temperature. The quality loss curve was in a state of abrupt decline while the temperature raised continuously from 156 °C onwards until it gradually smoothed out at a temperature of 471 °C. Compared with the CQDs, there was no mass loss below 373 °C depending on the TGA curve of PVP homopolymer, affirming that PVP exhibited a high degree of thermal stability. The curve stopped diverging after a sudden drop during a temperature of 373 to 471 °C, which suggested pyrolysis was fully underway. Combined with the curve of the CQDs@PVP association, it demonstrated two phases of variation. The thermal behavior of the initial stage, which exhibited a weight loss of 19 wt% in the same temperature range, was analogous to CQDs, and the second stage, which showed a quality loss of 68% followed a similar trend to PVP

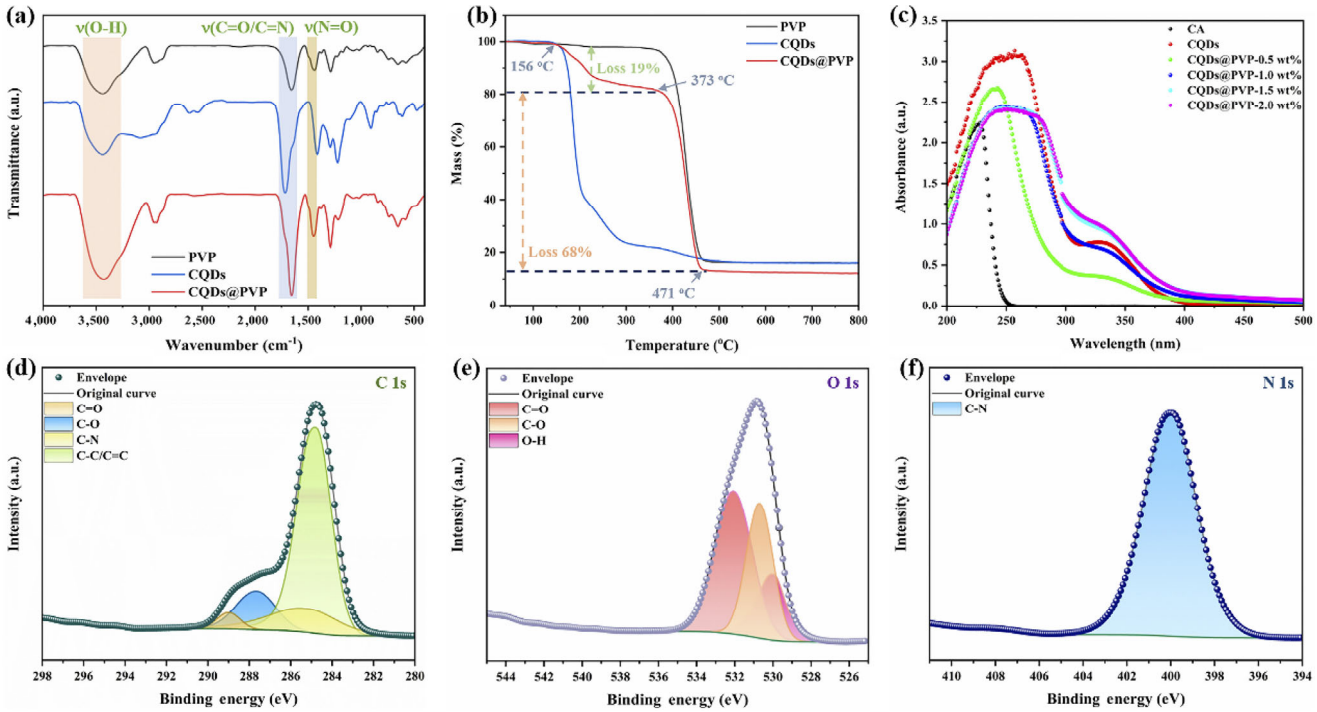


Fig. 2 (a) FTIR of the PVP, CQDs, and CQDs@PVP composite. (b) TGA curves of the PVP, CQDs, and CQDs@PVP composite. (c) UV-Vis curves of the CA and CQDs with 1.0 wt%, and various mass fractions with 0.5–2.0 wt% of CQDs@PVP in water. XPS spectrums of CQDs@PVP with (d) C 1s, (e) O 1s, and (f) N 1s.

homopolymer. Therefore, the curves of TGA validly proofed the successful modification of PVP by CQDs and the excellent thermal stability of CQDs@PVP composite materials.

The CQDs were obviously distinguished by their strong absorption peak in the UV region. As shown in Fig. 2(c), the curves of CQDs@PVP in water with various mass ratios in which the CA and CQDs were 1.0 wt% had observed by UV-Vis. The CA performed minimal absorption intensity below 230 nm as it was a colorless and transparent liquid. At the same time, the absorption peaks of CQDs and CQDs@PVP at 260 nm and 330 nm were ascribed to the $\pi \rightarrow \pi^*$ leap in the C=C bond and the $n \rightarrow \pi^*$ leap in the C=O bond excepted the 0.5 wt% CQDs@PVP, which exhibited an absorption peak at 240 nm and induced changes in energy differences due to small concentrations of CQDs spatial shape alterations [37]. The absorbance of curves at 330 nm showed an upward trend with increasing concentration, which was consistent with the actual theory. These results directly confirmed the successful preparation of CQDs and the similar properties of CQDs after modification.

The chemical structure of the CQDs@PVP association was further validated by XPS (Figs. 2(d)–2(f)). The atomic content of the CQDs@PVP composite, enriched with N element due to the PVP modification, is presented in Table S1 in the Electronic Supplementary Material (ESM). The C 1s, O 1s, and N 1s photoelectron spectra were aligned by 284.8, 531.0, and 400.0 eV, respectively, and the peak-differentiation-imitating was performed using Gauss-Lorentz hybrid algorithm [38]. There were four peaks of C 1s fine spectrum located at 289.1, 287.8, 285.5, and 285.1 eV ascribed to the C=O, C–O, C–N, and C–C/C=C bonds, respectively (Fig. 2(d)) [39]. In addition, the O 1s refined spectrum fitted by three peaks at 532.3, 530.7, and 530.0 eV, which suggested the existence of C=O, C–O, and O–H bonds, respectively (Fig. 2(e)). Compared with the CQDs monomer, the N element was visible and only a single peak attributed to the C–N bond was present in the N 1s spectrum (Fig. 2(f)). Therefore, the XPS fine spectrum of CQDs@PVP association were exactly matched to the FTIR, indicating that the PVP homopolymer were grafted on the surface of the CQDs.

3.2 Dispersion stability of the nano additives

Excellent dispersion of additives directly determines the tribological effect of the lubrication system. The dispersion stability of the prepared nanocomposite was observed by means of a standing experiment in Fig. 3. The 1.0 wt% CQDs, used as a comparison sample, and 0.5–2.0 wt% CQDs@PVP composite were observed in PEG400 (Fig. 3(a)) and water (Fig. 3(d)). Both CQDs and CQDs@PVP exhibited superior dispersibility in PEG400 and water, respectively, which was sonicated for 5 min prior to resting. Subsequently, the samples remained clear and transparent after 180 days in either PEG400 (Fig. 3(b)) or water (Fig. 3(e)) with absolutely no visible precipitation. Meanwhile, the bottom of the glass vial was observed after it had been turned upside down, and no precipitation of nanoparticles or impurities was found (Figs. 3(c) and 3(f)). These results were attributed to the polar hydroxyl or carboxyl bond in CQDs and the strongly polar lactam group in the modified PVP. Therefore, the superior friction and anti-wear properties of the base oil were closely related to the excellent dispersion stability of the additives.

3.3 High-temperature tribological properties of CQDs@PVP

To improve the high-temperature tribological properties of the base lubrication, both CQDs and CQDs@PVP nanoparticles were systematically studied in various concentrations and temperatures, respectively. As shown in Fig. 4(a), the blank curve exhibited a trend of increasing and then decreasing at 200 °C and 200 N in PEG400, in which the CoF of CQDs was smooth and generally higher than blank before 1,300 s. On the other hand, CQDs@PVP displayed a short fluctuating run-in period of 200s, followed by a gradual increase in CoF, which was overall lower than the blank. Meanwhile, the blank curve at 150 °C demonstrated an opposite trend to that observed at 200 °C (Fig. 4(b)). The CoF of CQDs, however, sharply increased and fluctuated dramatically during the friction process after 300 s. The friction coefficient of CQDs@PVP displayed a similar direction to 200 °C, indicating that it possessed the abilities of friction reduction and anti-wear at high temperatures.

To screen for the optimum additive dosage, it was tested for tribology with four concentrations (0.5–2.0 wt%) by means of a linear increase at 150 °C. The results, presented in Fig. 4(c), indicate that the average coefficient of friction of CQDs was lower than PEG400 but greater than CQDs@PVP at various concentrations. While the CoF of CQDs@PVP did not differ significantly from CQDs at other concentrations, it displayed an optimum average friction coefficient of 0.109 at 1.0 wt% over the entire sliding period.

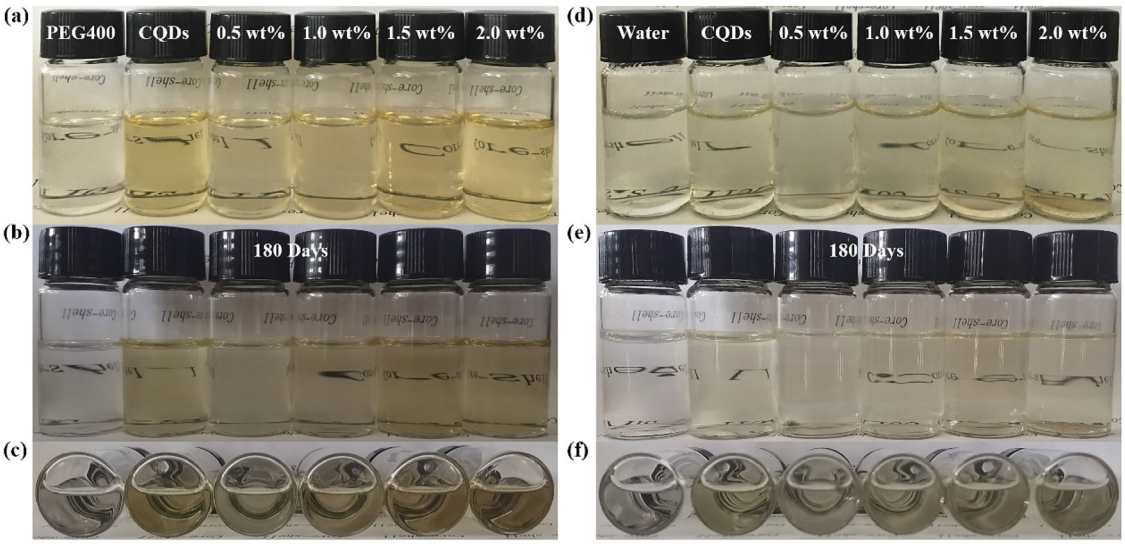


Fig. 3 Optical image of PEG, water, 1.0 wt% CQDs and 0.5–2.0 wt% CQDs@PVP static experiments. (a) Sonicated for 5 min in PEG400. (b) Standing after 180 days. (c) Bottom of glass bottle after inversion. (d) Sonicated for 5 min in water. (e) Standing after 180 days. (f) Bottom of glass bottle after inversion.

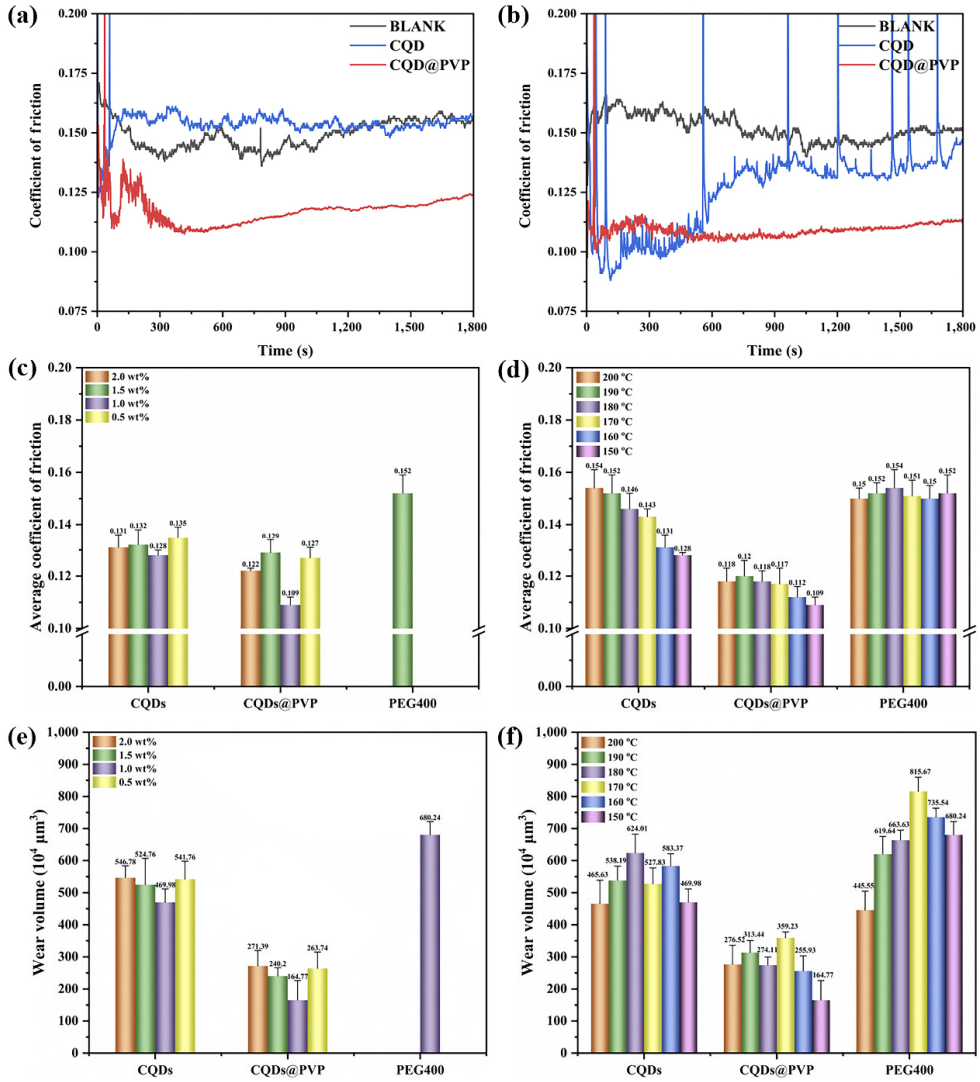


Fig. 4 Coefficient of friction curves for the PEG400 with 1.0 wt% CQDs and CQDs@PVP under set conditions (load: 200 N, frequency: 25 Hz, stroke: 1 mm, time: 30 min). (a) 200 °C, (b) 150 °C. The average coefficient of friction and wear volume under single change conditions. (c, e) 0.5–2.0 wt%, (d, f) 150–200 °C.

In other words, when the PVP homopolymers were grafted on the CQDs surface, it was efficient in strengthening friction reduction and anti-wear properties. The wear volume exhibited a similar pattern to the average friction coefficient at different concentrations, as shown in Fig. 4(e). In general, both CQDs and CQDs@PVP significantly decreased the wear volume, especially in the amount of 1.0 wt% CQDs@PVP, its wear volume was reduced by approximately 75.78% of PEG400 and 69.94% of CQDs. Therefore, the hydrogen-bonded connection of PVP via core-shell structures was found to be responsible for the synergistic effect that strengthened the tribological properties of CQDs [40].

In addition, the average coefficient friction and wear volume was investigated to inspect further the effect of high temperature (150–200 °C) tribological properties in PEG400, as shown in Figs. 4(d) and 4(f). For the CQDs and CQDs@PVP, the average coefficient friction generally exhibited a constantly decreasing trend as the temperatures continued to decline, in which the CQDs displayed a higher CoF than PEG400 at 200 °C (Fig. 4(d)). Simultaneously, the average coefficient friction of CQDs@PVP was lower than that of the PEG400 and CQDs at all temperatures, and especially at 150 °C, this was due to PVP protecting the CQDs from the inevitable thermal decomposition at high temperatures, which enabled sufficient CQDs

particles to be provided to form a strong protective film in the friction process. In contrast to the average coefficient friction, Fig. 4(f) demonstrated an increasing and then decreasing trend in wear volume as the temperature dropped. Furthermore, the CQDs@PVP possessed minimal wear volume loss at 150 °C, which suggested that the undecomposed CQDs possessed excellent film-forming ability, friction reduction and anti-wear potential under the condition of high temperature.

The tribological tests conducted in PEG400 revealed that the optimum addition of CQDs@PVP was 1.0 wt%, which was slected for subsequent tests. Because of the excellent hydrophilicity and dispersion stability of CQDs@PVP, its tribological properties in water at high temperatures were further studied. As shown in Figs. 5(a) and 5(b), tribological tests were carried out for 10 min at 90 and 80 °C because of the evaporation of the aqueous solution under high-temperature conditions. At the same time, the lubricant was not added further during the friction process to prevent changes in concentration from affecting the accuracy of the experiment. The friction coefficient curves of CQDs and CQDs@PVP were significantly lower than that of pure water, with a 44.23% reduction in the CoF at 90 °C, and the CQDs@PVP is consistently lower than CQDs to the end (Fig. 5(a)). Figure 5(b) exhibited a similar trend to 90 °C under 80 °C, but the curve of CQDs@PVP gradually raised after 250 s until it overtook CQDs, which was considered to be an increase in the CoF caused by the rising concentration of massive solvent evaporation. Figures 5(c)–5(e) showed the curve for a 30 min long grinding at 70–50 °C, which similarly displayed an active friction-reduction effect. In the same way, the CoF of CQDs@PVP remained lower than CQDs during the friction process except at the temperature of 70 °C, which may have been influenced by the testing environment. The wear volume of CQDs and CQDs@PVP exhibited a state that gradually decreased as the temperature dropped. Meanwhile, the lubricant with additives offered excellent anti-wear properties at different temperatures, reducing the wear volume by up to 79.68%. Based on these advantages, CQDs@PVP likewise exhibited excellent friction reduction and anti-wear properties in water.

3.4 Microscopic analysis of wear morphology

To observe and demonstrate the wear state of friction-pairs surface which could be reduced by

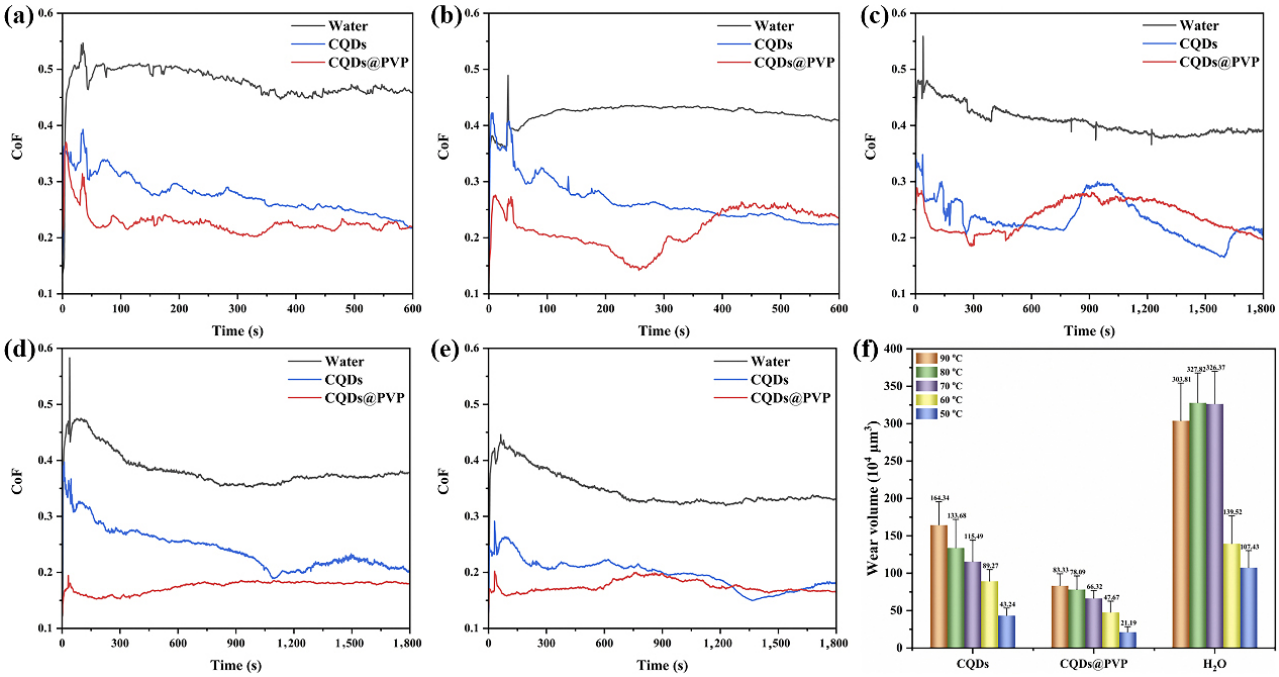


Fig. 5 CoF curves of water, CQDs, and CQDs@PVP at (a) 90 °C, (b) 80 °C, (c) 70 °C, (d) 60 °C, (e) 50 °C, and the corresponding (f) wear volume.

lubricants with additives at high temperatures, the wear tracks on steel discs and balls were examined by an optical microscope and non-contact 3D optical surface profilometer (Fig. 6). The PEG400 and its solution with CQDs were employed as lubrication materials, abrasion marks were inspected on the steel disc surface after tribological test, and wear widths were 824.45 and 749.62 μm, respectively (Figs. 6(a) and 6(b)). Conversely, a wear track that exhibited less and slight scars compared to the comparative samples was recorded on the surface of the steel disc lubricated by CQDs@PVP solution, and the width was 551.32 μm (Fig. 6(c)). Moreover, the worn profiles of 3D contours further validated the correctness of the results, and the abrasion depths were 14.35, 12.63, and 1.91 μm (Figs. 6(d)–6(i)). On the face of it, the CQDs@PVP solution effectively inhibited direct contact of the steel tribopairs and helped to create a homogeneous lubrication film on the surface of the disc [41]. In the meantime, the wear spot diameters of steel balls surface were observed after the friction test, with values of 794.82, 856.22, and 728.78 μm for PEG400, CQDs, and CQDs@PVP, respectively.

The worn morphology of water, CQDs and CQDs@PVP solution were investigated and characterized by the same means, as shown in Fig. S1 in the ESM. After the 50 °C friction experiment, the surface of steel disc remained black impurities and marks, which were attributed to the corrosion of the steel block surface by water at high temperature (Fig. S1(a) in the ESM). In the same way, the disc surface of the CQDs solution also appeared with some black traces on the left side of the wear scar, suggesting that CQDs were unable to completely

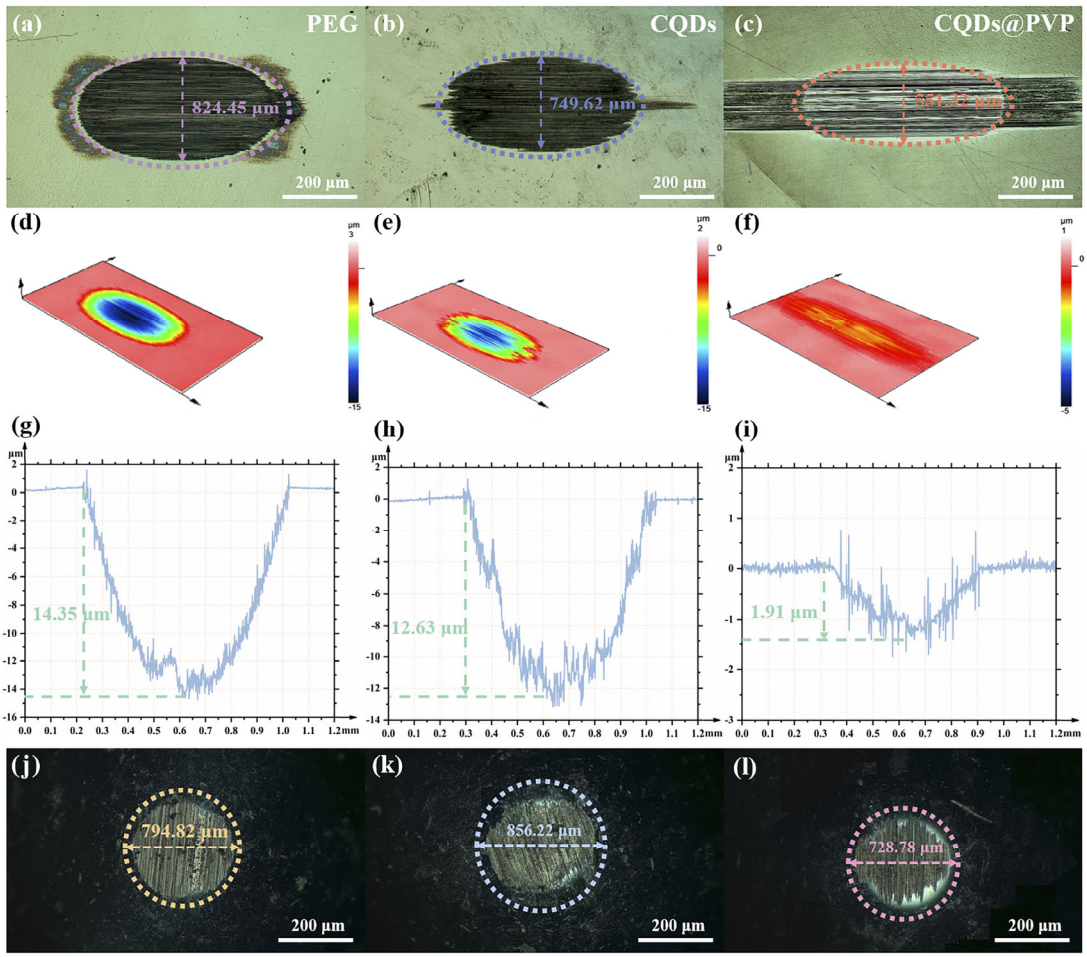


Fig. 6 Physical morphologies of steel discs by PEG400, CQDs and CQDs@PVP. (a–c) Optical micrographs, (d–f) 3D morphologies, and (g–i) depth. (g–l) Worn diameters of steel balls corresponded to discs by optical microscope. The test conditions were temperature 150 °C, load 200 N, frequency 25 Hz, stroke 1 mm, and time 30 min.

eradicate the effects of high temperature (Fig. S1(b) in the ESM). In contrast, a relatively clean wear mark was noted on the surface of the steel disc lubricated by CQDs@PVP solution (Fig. S1(c) in the ESM) and displayed width of worn (834.01 μm) that was smaller than pure water (927.31 μm) and larger than CQDs solution (635.71 μm), but the depths of solutions were 6.61, 3.59, and 1.12 μm (Figs. S1(d)–S1(i) in the ESM), respectively. Furthermore, the scar diameters of the steel balls surface were 685.72, 854.21, and 310.08 μm, respectively, which exhibited the opposite trend to the disc and suggested the uncertainty of steel ball wear mark after friction tests (Figs. S1(g)–S1(l) in the ESM). In summary, the CQDs@PVP was effective in both PEG400 and water to reduce frictional wear and achieve high-temperature anti-wear.

To further investigate the worn status of CQDs@PVP, the wear scars were characterized by FE-SEM and the respective element distribution on the steel disc was recorded by EDS (Fig. 7). As shown in Fig. 7(a), the large deep grooves and light furrows appeared on the wear scars of tribopair, after 30 min of rubbing by PEG400, which also exhibited in the red illustration. Meanwhile, the elements of C and O clearly clustered on the wear scar, demonstrating the ability of PEG400 to adsorb in the contact zone for chemical reactions (Figs. 7(d)–7(g)). Moreover, the handful deep grooves and light furrows displayed on the surface of wear trace by the friction of CQDs solution, and the high magnification electron micrograph of the red selected area also showed the corresponding morphology (Fig. 7(b)). The element of C, which was less content and O equally enriched on the wear surface, and the reasons for the small amount of C may be ascribed to the thermal decomposition of CQDs at high temperature and the inability to form a reaction film on the tribopair (Figs. 7(h)–7(k)) [42]. Compared with both PEG400 and CQDs solution, it failed to find roughness on the surface of the steel block, and only light abrasion was visible, which suggested the excellent effect of the anti-wear property of CQDs@PVP. In addition, the wear scar exhibited no significant

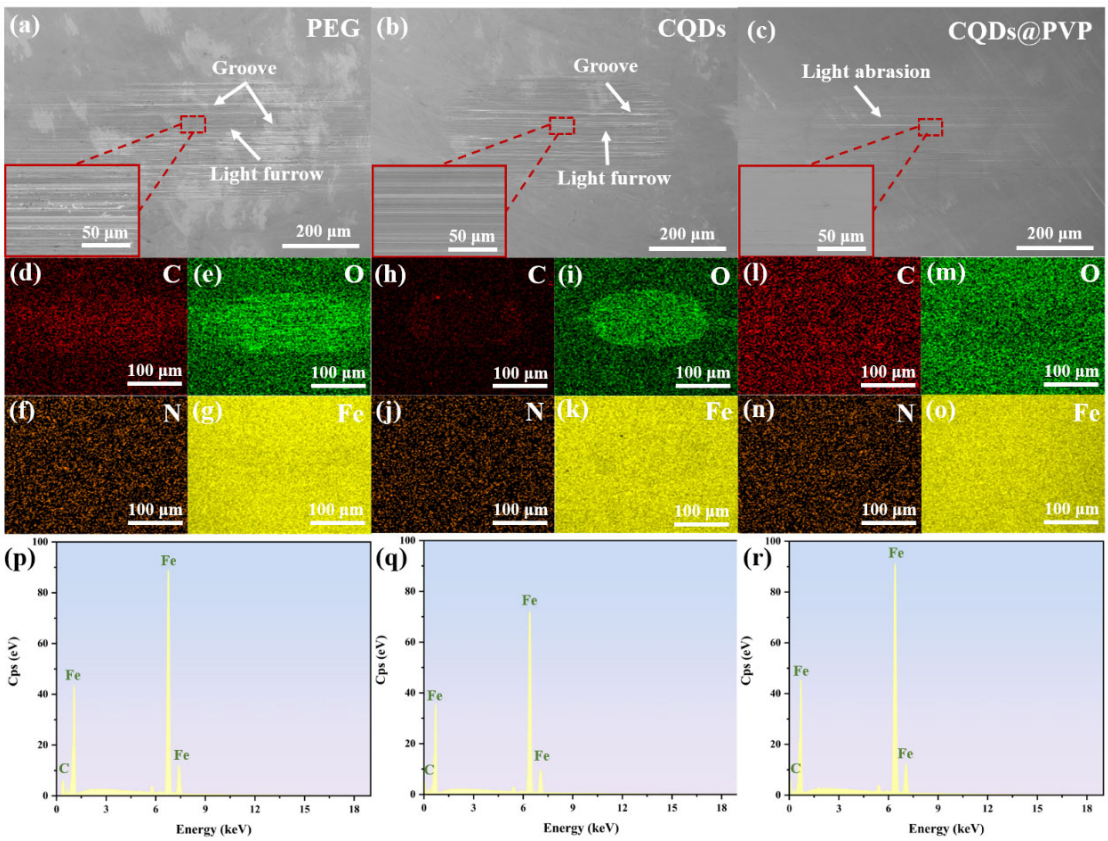


Fig. 7 SEM images of the wear scars on the steel discs. (a) PEG400, (b) CQDs and (c) CQDs@PVP. The element distribution of (d, h, l) C, (e, i, m) O, (f, j, n) N, and (g, k, o) Fe after the friction test. (p–r) Content of each element.

aggregation of elements C and O, which may be attributed to the minor wear resulting in conspicuous elemental aggregation. The elemental content of the individual wear spots after friction was also indicated by Figs. 7(p)–7(r). Moreover, Fig. S2 in the ESM in water also showed a similar abrasion morphology to Fig. 7 and the distribution of elements, except for the distribution of element C in CQDs@PVP, which exhibited concentrated behavior, suggesting that CQDs@PVP had tribofilm formation on the surface of the tribopair. Therefore, the CQDs@PVP solution was able to reduce abrasion and react to form a film.

3.5 The lubrication mechanism analysis

The lubrication mechanism of CQD@PVP revealed by Raman analysis of the steel block surface after high-temperature friction, as shown in Fig. 8(a). The peaks of CQDs@PVP at 1,580 and 1,360 cm^{-1} correspond to G and D, respectively, indicating the formation of carbon film on wear surface [42]. Furthermore, both peaks of 863 and 617 cm^{-1} were attributed to the C–O–C and Fe–O [43, 44]. Compared with the PEG400, the absence of G and D peaks in CQDs indicated the presence of Fe–O groups, implying the occurrence of tribo-chemical reactions during the friction process and the simple deposition of PEG400 on the steel disc surface.

Based on the results of Raman, the XPS spectra were used further to characterize the chemical state of the worn surface and prove the possible lubrication mechanism of CQDs@PVP (Figs. 8(b)–8(f)). The different intensities of C 1s (284.8 eV), O 1s (531.0 eV), N 1s (400.0 eV), and Fe 2p (720.0 eV) were observed by survey and charge calibrated with C 1s, smoothed and fitted by Gaussian–Lorentzian to separate the peaks (Fig. 8(b)) [45]. As shown in Fig. 8(c), the four peaks of C 1s at 284.79, 285.54, 286.39, and 288.61 eV were attributed to the C–C/C=C, C–H/C–N, C–O, and C=O bonds, respectively, which was related to the deposition of CQDs@PVP on the wear surface to produce a carbon film during friction [32, 46]. In the spectrum of O 1s, peaks located at 529.75, 531.20, and 532.50 eV demonstrated the presence of C=O, C–O, and Fe–O bonds, respectively [47, 48]. Meanwhile, the N 1s only exhibited one peak at 399.81 eV, which was ascribed to the C–N bond. Most of these chemical groups were derived from the deposition of CQDs@PVP and PEG400. The Fe 2p peaks appeared at 711.30 (Fe $2p_{1/2}$), 713.50 (Fe^{3+}), and 724.83 eV (Fe^{2+}), indicating the chemical reaction that occurred during

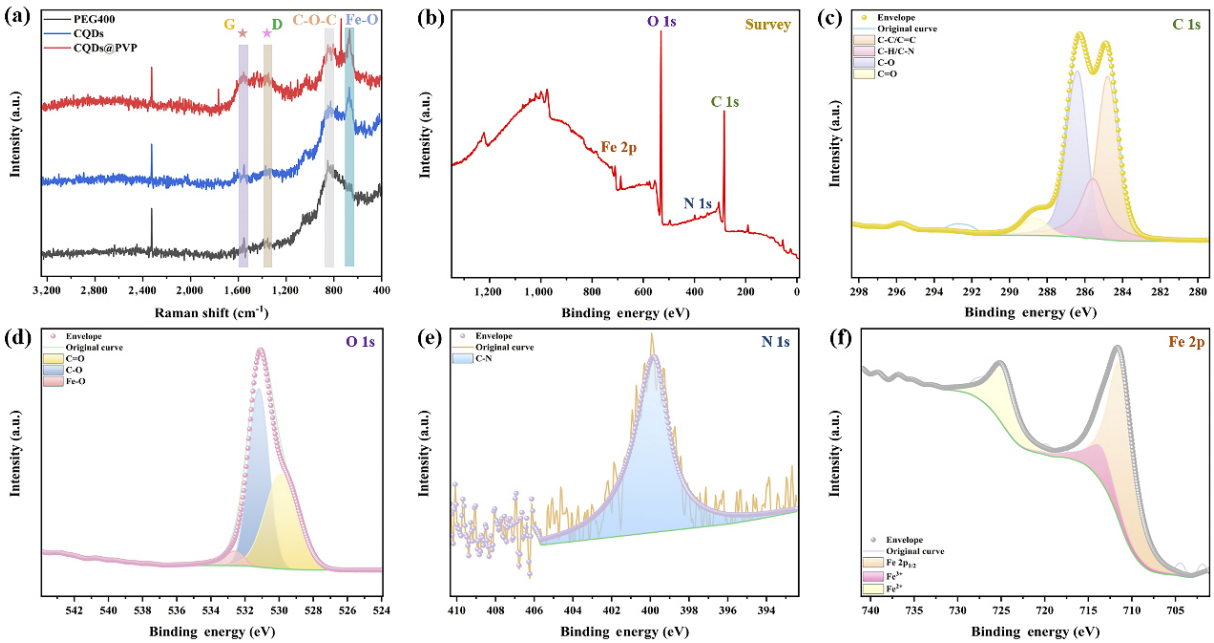


Fig. 8 (a) Raman spectra of the wear scars by PEG400, CQDs, and CQDs@PVP lubricated. XPS spectrum on the worn surface after CQDs@PVP lubrication. (b) Survey, (c) C 1s, (d) O 1s, (e) N 1s, and (f) Fe 2p. The test conditions were: 150 °C, 200 N, 1 mm, 25 Hz, and 30 min.

the friction process to create a reaction film of iron oxide compounds [6]. As shown in Fig. S3 in the ESM, CQDs@PVP exhibited a similar XPS spectrum to PEG in water, indicating the same formation of a chemically reactive film. In summary, the carbon film formed by the deposition of CQDs@PVP on the worn surface and the tribo-chemical film created by the oxidation of iron were the main factors that effectively enhanced the tribological properties of the base oil.

Based on characterization results, including EDS, Raman, XPS and tribological properties, the lubrication mechanism of CQDs@PVP material is presented, and the schematic diagram is described in Fig. 9. When the lubrication of CQDs@PVP solution is plastered on the tribopair surface, the steel block is partially filled with 3 nm nanoparticles in the solvent to improve the surface roughness and prevent increased wear caused by direct contact with sharp parts during friction. Meanwhile, several CQDs@PVP nanoparticles are deposited on the surface of the steel disc with the lubricant, reducing the frictional resistance of the friction pairs. As the friction proceeds over a long period of time, the nanoparticles are gradually extruded into a laminar structure while acting as ball bearings and flattening out on the surface of the steel block, and progressively forming a deposited film consisting mainly of additives [49]. Furthermore, the additive interacts with the iron during the friction process and constitutes a chemical reaction film under the influence of air at high temperatures, effectively improving the interfacial action between the friction pairs and enhancing the tribological properties of the lubricant in terms of friction reduction and anti-wear [50].

4 Conclusions

Although the tribological properties of CQDs nanomaterials have been extensively investigated, their performances as high-temperature resistant lubricant additives have received limited attention in the literature. The grafting of homopolymers on the surface of CQDs nanomaterials has been found to exhibit superior performance compared to the application of carbon quantum dots individually, and the conclusions are as follows:

(1) The PVP is attached to the CQDs surface by hydrogen bonding, forming CQDs@PVP nanoparticles with a lattice spacing of 0.21 nm and an average diameter of 3.0 nm. Various physicochemical techniques have further characterized the core–shell structure and chemical modifications of the material.

(2) CQDs@PVP, as a lubrication additive, is stable in PEG400 and water for 180 days without precipitation, indicating its well-defined amphiphilic properties. Meanwhile, it exhibits excellent friction and wear reduction properties under high-temperature conditions (150–200 °C).

(3) The synergistic effect of CQDs and PVP imparts a dense carbon film at the friction interface, while the iron compounds also constitute a chemically reactive film during the friction process. These two lubrication films interact synergistically to prevent damage to the friction substrate and achieve excellent lubrication properties.

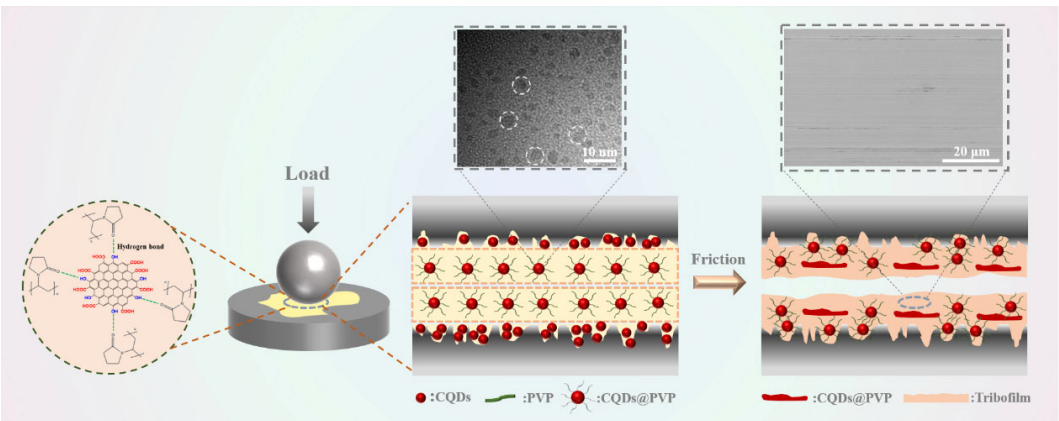


Fig. 9 Diagram of the lubrication mechanism of CQDs@PVP as an additive.

Acknowledgements

This work was financially supported by the Strategic Priority Research Program of the Chinese Academy of Sciences (No. XDB 0470301), the Key R&D Program of Shandong Province (Nos. 2020CXGC011002 and 2022CXGC020309), and the National Natural Science Foundation of China (No. 51975560).

Declaration of competing interest

The authors have no competing interests to declare that are relevant to the content of this article.

Electronic Supplementary Material: Supplementary material is available in the online version of this article at https://doi.org/10.1007/s40544-024-0871-x.

Open Access This article is licensed under a Creative Commons Attribution 4.0 International License, which permits use, sharing, adaptation, distribution and reproduction in any medium or format, as long as you give appropriate credit to the original author(s) and the source, provide a link to the Creative Commons licence, and indicate if changes were made.

The images or other third party material in this article are included in the article's Creative Commons licence, unless indicated otherwise in a credit line to the material. If material is not included in the article's Creative Commons licence and your intended use is not permitted by statutory regulation or exceeds the permitted use, you will need to obtain permission directly from the copyright holder.

To view a copy of this licence, visit http://creativecommons.org/licenses/by/4.0/.

References

[1] Zhao J, Huang Y Y, He Y Y, Shi Y J. Nanolubricant additives: A review. *Friction* **9**(5): 891–917 (2021)

[2] Meng Y G, Xu J, Ma L R, Jin Z M, Prakash B, Ma T B, Wang W Z. A review of advances in tribology in 2020–2021. *Friction* **10**(10): 1443–1595 (2022)

[3] Xiang Z F, Liu X B, Ren J, Luo J, Shi S H, Chen Y, Shi G L, Wu S H. Investigation of laser cladding high temperature anti-wear composite coatings on Ti_6Al_4V alloy with the addition of self-lubricant CaF_2. *Appl Surf Sci* **313**: 243–250 (2014)

[4] Gong K L, Lou W J, Zhao G Q, Wu X H, Wang X B. MoS_2 nanoparticles grown on carbon nanomaterials for lubricating oil additives. *Friction* **9**(4): 747–757 (2021)

[5] Wu X H, Gong K L, Zhao G Q, Lou W J, Wang X B, Liu W M. Mechanical synthesis of chemically bonded phosphorus–graphene hybrid as high-temperature lubricating oil additive. *RSC Adv* **8**(9): 4595–4603 (2018)

[6] Liu H C, Wang X Y, Yang T, Su H G, Wang X B, Zhang S M, Lou W J. Rheological behaviors and tribological properties of nano-silica grease: A study compared with lithium grease and polyurea grease. *Tribol Int* **186**: 108657 (2023)

[7] Yang T, Zhao Q, Hu M, Wang X Z, Zhao G Q, Gong K L, Wang X B. Tribological behavior of novel core–shell Fe_3O_4@PEG nano-additives. *Tribol Lett* **70**(4): 116 (2022)

[8] Padgurskas J, Rukuiza R, Prosyčevas I, Kreivaitis R. Tribological properties of lubricant additives of Fe, Cu and Co nanoparticles. *Tribol Int* **60**: 224–232 (2013)

[9] Mosey N J, Müser M H, Woo T K. Molecular mechanisms for the functionality of lubricant additives. *Science* **307**(5715): 1612–1615 (2005)

[10] Zhang L, Xie G X, Wu S, Peng S G, Zhang X Q, Guo D, Wen S Z, Luo J B. Ultralow friction polymer composites incorporated with monodispersed oil microcapsules. *Friction* **9**(1): 29–40 (2021)

[11] Gong K L, Lou W J, Zhao G Q, Wu X H, Wang X B. Investigation on tribological behaviors of MoS_2 and WS_2 quantum dots as lubricant additives in ionic liquids under severe conditions. *Friction* **8**(4): 674–683 (2020)

[12] Gong K L, Wu X H, Zhao G Q, Wang X B. Tribological properties of polymeric aryl phosphates grafted onto multi-walled carbon nanotubes as high-performances lubricant additive. *Tribol Int* **116**: 172–179 (2017)

[13] Xia Y Q, Wang Y H, Hu C L, Feng X. Conductivity and tribological properties of IL-PANI/WS_2 composite material in lithium complex grease. *Friction* **11**(6): 977–991 (2023)

[14] Shang W J, Cai T, Zhang Y X, Liu D, Sun L W, Su X Y, Liu S G. Covalent grafting of chelated othoborate ionic liquid on carbon quantum dot towards high performance additives: Synthesis, characterization and tribological evaluation. *Tribol Int* **121**: 302–309 (2018)

[15] Shu Y, Ye Q Y, Dai T, Xu Q, Hu X Y. Encapsulation of luminescent guests to construct luminescent metal–organic frameworks for chemical sensing. *ACS Sens* **6**(3): 641–658 (2021)

[16] Khan M E, Mohammad A, Yoon T. State-of-the-art

developments in carbon quantum dots (CQDs): Photo-catalysis, bio-imaging, and bio-sensing applications. *Chemosphere* **302**: 134815 (2022)

[17] Zhang M, Wang W T, Zhou N L, Yuan P, Su Y T, Shao M N, Chi C, Pan F Y. Near-infrared light triggered photo-therapy, in combination with chemotherapy using magnetofluorescent carbon quantum dots for effective cancer treating. *Carbon* **118**: 752–764 (2017)

[18] Roy A, Samanta S, Singha K, Maity P, Kumari N, Ghosh A, Dhara S, Pal S. Development of a thermoresponsive polymeric composite film using cross-linked β-cyclodextrin embedded with carbon quantum dots as a transdermal drug carrier. *ACS Appl Bio Mater* **3**(5): 3285–3293 (2020)

[19] Tang W W, Zhang Z, Li Y F. Applications of carbon quantum dots in lubricant additives: A review. *J Mater Sci* **56**(21): 12061–12092 (2021)

[20] El-Shamy A G, Zayied H S S. New polyvinyl alcohol/carbon quantum dots (PVA/CQDs) nanocomposite films: Structural, optical and catalysis properties. *Synth Met* **259**: 116218 (2020)

[21] Kavitha R, Nithya P M, Girish Kumar S. Noble metal deposited graphitic carbon nitride based heterojunction photocatalysts. *Appl Surf Sci* **508**: 145142 (2020)

[22] Liu G Q, Feng Y, Gao X H, Chen Z, Zhao N, Zhou F, Liu W M. Synovial fluid-inspired biomimetic lubricating microspheres: Zwitterionic polyelectrolyte brushes-grafted microgels. *Friction* **11**(6): 938–948 (2023)

[23] Wang J H, Li X R, Deng Y Y, Chen S H, Liang W F, Zhang L X, Wei X Y, Gao S Y, Wan Y. Carbon quantum dots doped with silver as lubricating oil additive for enhancing tribological performance at various temperatures. *Appl Surf Sci* **599**: 154029 (2022)

[24] Wang F, Shang L L, Zhang G G, Wang Z F. Polyethylene glycol derived carbon quantum dots nanofluids: An excellent lubricant for diamond-like carbon film/bearing steel contact. *Friction* **10**(9): 1393–1404 (2022)

[25] Wang H S, Qiao X L, Chen J G, Wang X J, Ding S Y. Mechanisms of PVP in the preparation of silver nanoparticles. *Mater Chem Phys* **94**(2–3): 449–453 (2005)

[26] Zhao C D, Cheng H, Jiang P F, Yao Y J, Han J. Preparation of lutein-loaded particles for improving solubility and stability by Polyvinylpyrrolidone (PVP) as an emulsion-stabilizer. *Food Chem* **156**: 123–128 (2014)

[27] Wang G S, Ma Y Y, Mu J B, Zhang Z X, Zhang X L, Zhang L N, Che H W, Bai Y M, Hou J X, Xie H L. Monodisperse polyvinylpyrrolidone-coated $CoFe_2O_4$ nanoparticles: Synthesis, characterization and cytotoxicity study. *Appl Surf Sci* **365**: 114–119 (2016)

[28] Rubio-Valle J F, Sánchez M C, Valencia C, Martín-Alfonso J E, Franco J M. Electrohydrodynamic processing of PVP-doped kraft lignin micro- and nano-structures and application of electrospun nanofiber templates to produce oleogels. *Polymers* **13**(13): 2206 (2021)

[29] Kaneda Y, Tsutsumi Y, Yoshioka Y, Kamada H, Yamamoto Y, Kodaira H, Tsunoda S I, Okamoto T, Mukai Y, Shibata H, *et al*. The use of PVP as a polymeric carrier to improve the plasma half-life of drugs. *Biomaterials* **25**(16): 3259–3266 (2004)

[30] Guo Y, Hao Z X, Wan C. Tribological characteristics of polyvinylpyrrolidone (PVP) as a lubrication additive for artificial knee joint. *Tribol Int* **93**: 214–219 (2016)

[31] Wang Y F, Hu A G. Carbon quantum dots: Synthesis, properties and applications. *J Mater Chem C* **2**(34): 6921 (2014)

[32] Wang H C, Li Y, Zhang S W, Che Q L, Hu L T, Zhang J J. Outstanding lubrication properties of carbon dot-based ionic liquids. *J Mol Liq* **376**: 121458 (2023)

[33] Zhang D Y, Chao D Y, Yu C Y, Zhu Q, Zhou S H, Tian L, Zhou L. One-step green solvothermal synthesis of full-color carbon quantum dots based on a doping strategy. *J Phys Chem Lett* **12**(37): 8939–8946 (2021)

[34] Subramani M S, Chatterjee S, Mohanta K. Nanoelectronic applications of carbon quantum dots. In: *Carbon Quantum Dots for Sustainable Energy and Optoelectronics.* Batabyal S K Pradhan B, Mohanta K, Bhattacharjee R R, Banerjee A, Ed. Woodhead Publishing, 2023: 183–203.

[35] Han G D, Cai J H, Liu C F, Ren J L, Wang X H, Yang J, Wang X Y. Highly sensitive electrochemical sensor based on xylan-based Ag@CQDs-rGO nanocomposite for dopamine detection. *Appl Surf Sci* **541**: 148566 (2021)

[36] Zheng Z W, Liu X L, Huang G W, Chen H J, Yu H X, Feng D P, Qiao D. Macroscale superlubricity achieved via hydroxylated hexagonal boron nitride nanosheets with ionic liquid at steel/steel interface. *Friction* **10**(9): 1365–1381 (2022)

[37] Riaz R, Ali M, Maiyalagan T, Anjum A S, Lee S, Ko M J, Jeong S H. Dye-sensitized solar cell (DSSC) coated with energy down shift layer of nitrogen-doped carbon quantum dots (N-CQDs) for enhanced current density and stability. *Appl Surf Sci* **483**: 425–431 (2019)

[38] Du C H, Yu T T, Zhang L Q, Shen R L, Wu Z S, Li X J, He X J, Feng Y G, Wang D A. Robust and universal macroscale superlubricity with natural phytic acid solutions. *Tribol Int* **183**: 108387 (2023)

[39] Du C H, Yu T T, Wu Z S, Zhang L Q, Shen R L, Li X J, Feng M, Feng Y G, Wang D A. Achieving macroscale

superlubricity with ultra-short running-in period by using polyethylene glycol-tannic acid complex green lubricant. *Friction* **11**(5): 748–762 (2023)

[40] Yang Y W, Yang G C, Hou K M, Wang H G, Wang N, Yang S R, Wang J Q. Environmentally-adaptive epoxy lubricating coating using self-assembled pMXene@ polytetrafluoroethylene core-shell hybrid as novel additive. *Carbon* **184**: 12–23 (2021)

[41] He J Q, Sun J L, Choi J, Wang C L, Su D X. Synthesis of N-doped carbon quantum dots as lubricant additive to enhance the tribological behavior of MoS_2 nanofluid. *Friction* **11**(3): 441–459 (2023)

[42] Tu Z Q, Hu E Z, Wang B B, David K D, Seeger P, Moneke M, Stengler R, Hu K H, Hu X G. Tribological behaviors of Ni-modified citric acid carbon quantum dot particles as a green additive in polyethylene glycol. *Friction* **8**(1): 182–197 (2020)

[43] Liu Y Q, Xu Y, Yan Y Z, Hu D D, Yang L Z, Shen R L. Application of Raman spectroscopy in structure analysis and crystallinity calculation of corn starch. *Starch Stärke* **67**(7–8): 612–619 (2015)

[44] Li Y T, Li H, Fan X Q, Xu X J, Zhu M H. Oil-soluble deep eutectic solvent as high-performance green lubricant additives for PAO 40 and PEG 200. *Tribol Int* **186**: 108602 (2023)

[45] Du C H, Yu T T, Zhang L Q, Deng H Y, Shen R L, Li X J, Feng Y G, Wang D A. Macroscale superlubricity with ultralow wear and ultrashort running-In period (~1 s) through phytic acid-based complex green liquid lubricants. *ACS Appl Mater Interfaces* **15**(7): 10302–10314 (2023)

[46] Xiao H P, Liu S H, Xu Q, Zhang H. Carbon quantum dots: An innovative additive for water lubrication. *Sci China Technol Sci* **62**(4): 587–596 (2019)

[47] Xue S H, Cui Y H, Chen X, Shi J Q, Liu S J, Ye Q, Zhou F. Zwitterionic dopamine sulfonate functionalized carbon quantum dots as water-based lubricant additive for friction and wear reduction. *Appl Surf Sci* **615**: 156411 (2023)

[48] Liu H C, Wang X Y, Zhao Q, Su H G, Wang X B, Zhang S M, Lou W J. Effect of temperature on rheological behaviors and tribological properties of nano-silica greases prepared from base oils with different viscosities. *Tribol Lett* **71**(2): 34 (2023)

[49] Wu X H, Gong K L, Zhao G Q, Lou W J, Wang X B, Liu W M. Surface modification of MoS_2 nanosheets as effective lubricant additives for reducing friction and wear in poly-α-olefin. *Ind Eng Chem Res* **57**(23): 8105–8114 (2018)

[50] Zhang W L, Li T H, An R, Wang J, Tian Y. Delivering quantum dots to lubricants: Current status and prospect. *Friction* **10**(11): 1751–1771 (2022)



Tao YANG. He received his bachelor degree (2020) in metallurgical from Northeastern University in China. He is currently a Ph.D. candidate in State Key Laboratory of Solid Lubrication, Lanzhou Institute of Chemical Physics (LICP), Chinese Academy of Sciences (CAS). His research focuses on intelligent nano-additives for lubricating oil.



Xiaozhen WANG. He received his master degree from the National Center of International Joint Research for Hybrid Materials in 2021 from Qingdao University. His current scientific interests are focused on lubricating oil addtive and its high-temperature application.



Yongmin LIANG. He is a full professor at the College of Chemistry and Chemical Engineering, Lanzhou University. He received his Ph.D. degree in organic chemistry from State Key Laboratory of Solid Lubrication, Lanzhou Institute of Chemical Physics (LICP), Chinese Academy of Sciences (CAS) in 2006. His research interests include metal organic chemistry, modern organic synthesis methods and applications of new functional organic materials. He has published more than 100 peer-reviewed journal papers.



Xiaobo WANG. He is a full professor in State Key Laboratory of Solid Lubrication, Lanzhou Institute of Chemical Physics (LICP), Chinese Academy of Sciences (CAS). He received his Ph.D. degree in physical chemistry from LICP in 2004. His research interest includes lubricating oils and greases, nano-additives, and tribology mechanism. He has published more than 200 peer-reviewed journal papers and been authorized 20 patents.